A Meshless MQ-RBF Approach with Artificial Viscosity for Shock-Resolved Shallow Water Flow Simulation

Marwane Bensaad[1*], Youssef Es-Sabry[1], and Elmiloud Chaabelasri[1]

[1] LPTPME, Faculty of Sciences, University Mohammed the first, Oujda 60000, Morocco
* Corresponding author: marwan.19.bens@gmail.com

Abstract. In this study, we introduce a meshless computational framework for simulating shallow water flows with shock phenomena using multiquadric radial basis functions (MQ-RBFs). The method approximates spatial derivatives through global collocation without relying on traditional mesh generation. To enhance stability and accurately resolve discontinuities such as hydraulic jumps and oblique shock waves, an artificial viscosity term is incorporated into the momentum equations. Time integration is performed using a second-order Runge-Kutta scheme, offering a balance between accuracy and computational efficiency. The model is validated through several benchmark test cases commonly encountered in hydraulic modeling. Results demonstrate strong agreement with analytical, experimental, and numerical reference solutions, highlighting the method's robustness and precision in capturing complex flow behavior.

Keywords: Meshless Numerical Scheme, Multiquadric Radial Basis Functions, Artificial Viscosity Stabilization, Shock Resolution, Shallow Water Flow Simulation, Runge-Kutta Time Integration, Hydraulic Discontinuities.

1 Introduction

Classical numerical schemes such as the finite difference method (FDM), the finite element method (FEM), and the finite volume method (FVM) have long been employed to solve shallow water equations (SWEs) in hydraulics and environmental flow modeling. While these mesh-based techniques are widely used, they encounter limitations when applied to flows characterized by discontinuities or complex geometries. In particular, the need for grid generation and connectivity makes them less flexible for problems involving irregular domains or shock phenomena. To address such challenges, shock-capturing strategies were incorporated into finite volume formulations, enabling reliable predictions of hydraulic jumps, dam-break flows, and open-channel transitions [1], [2], [3], [4], [5], [6], [7], [8], [9]. Despite these advances, the dependence on structured or unstructured meshes continues to restrict their adaptability and computational efficiency in certain scenarios.

In recent years, meshless approaches have emerged as robust alternatives to classical discretization schemes [10], [11], [12], [13]. These methods eliminate the requirement for predefined connectivity between nodes, offering greater flexibility for modeling free-surface flows over irregular terrains. Among meshless techniques, the radial basis function (RBF) collocation method introduced by Kansa [14] has attracted significant attention. Variants of the method have been applied to diverse problems in fluid dynamics, pollutant transport, and hydraulic simulations [12], [13], [15], [16]. Nevertheless, one of the main issues associated with RBF formulations is the occurrence of spurious oscillations in high-gradient regions, especially near shocks or discontinuities [17], [18].

The present work introduces a meshless framework based on multiquadric radial basis functions (MQ-RBFs) coupled with an artificial viscosity stabilization technique. This combination is designed to suppress non-physical oscillations while retaining the high accuracy of the RBF collocation method, extending earlier efforts by Chaabelasri [9], [16] and others [12], [15]. Unlike previous RBF-based studies, which either focused on smooth flows or employed limited stabilization, our contribution explicitly targets shock-resolved SWE simulations with complex flow regimes. The method is validated through benchmark cases involving oblique hydraulic jumps, supercritical flows in converging channels, and transcritical flows over irregular beds. In each case, the proposed scheme demonstrates strong agreement with reference data while preserving the robustness of meshless formulations.

The novelty of this study lies in (i) applying MQ-RBF with artificial viscosity for two-dimensional SWE problems involving hydraulic shocks, (ii) improving stability without sacrificing accuracy, and (iii) showing that the method performs competitively with traditional FVM solvers [3], [4], [5], [6], [7], [8] while avoiding mesh-related complexities. These contributions position the MQ-RBF scheme as a promising alternative for complex hydraulic simulations where mesh generation is impractical or costly.

2 Governing Equations and Boundary Conditions

2.1 Shallow water equations

The behavior of shallow water flow finds representation through the utilization of shallow water equations (SWEs). These equations are obtained by depth-averaging the incompressible Navier–Stokes equations under the hydrostatic pressure assumption [7], [19]. They are widely applied in river hydraulics, coastal flows, flood routing, and dam-break problems. In conservative form, the two-dimensional SWE system can be written as:

$$\frac{\partial W}{\partial t}+\frac{\partial F(W)}{\partial x}+\frac{\partial G(W)}{\partial y}=S(W) \tag{1}$$

Where

$$W=\begin{bmatrix} h \\ q_x \\ q_y \end{bmatrix},\ F(W)=\begin{bmatrix} q_x \\ \frac{q_x^{\,2}}{h}+\frac{1}{2}gh^2 \\ \frac{q_x q_y}{h} \end{bmatrix},\ G(W)=\begin{bmatrix} q_y \\ \frac{q_x q_y}{h} \\ \frac{q_x^{\,2}}{h}+\frac{1}{2}gh^2 \end{bmatrix}, \tag{2}$$

Here, h denotes the water depth, while $q_x = hu \ and \ q_y = hv$ represent the discharges in the x- and y-directions. The depth-averaged velocities are u and v. The source term S(W) accounts for bottom topography $S_b(W)$ and frictional effects $S_f(W)$:

$$S(W)=S_b(W)+S_f(W) \tag{3}$$

With

$$S_b(W)=\begin{bmatrix} 0 \\ -gh\partial_x z \\ -gh\partial_y z \end{bmatrix},\ S_f(W)=\begin{bmatrix} 0 \\ -gh\tau_x \\ -gh\tau_y \end{bmatrix} \tag{4}$$

where z(x,y) is the bed elevation and $\tau_x \ and \ \tau_y$ are the bottom friction stresses. In hydraulic modeling, these stresses are often expressed using Manning's law:

$$\tau_x=\frac{\eta^2 q_x\sqrt{q_x^{\,2}+q_y^{\,2}}}{h^{\frac{10}{3}}},\ \tau_y=\frac{\eta^2 q_y\sqrt{q_x^{\,2}+q_y^{\,2}}}{h^{\frac{10}{3}}} \tag{5}$$

with Manning's roughness coefficient denoted by η.
This formulation is consistent with widely used SWE representations in open-channel hydraulics [20], [21].

2.2 Boundary conditions

Different boundary conditions are required depending on the physical configuration. In this study, two types are applied:

- **Transmissive boundaries**: used to represent open inflow and outflow. Flow variables at the boundary are extrapolated from interior points normal to the boundary, ensuring minimal wave reflection.

- **Reflective boundaries**: used for solid walls. Here, normal velocity components are set to zero at the boundary, while tangential components are preserved, effectively imposing a slip condition.

These treatments follow standard hydraulic modeling practices [22], [23], [24].

In the context of a meshless RBF collocation scheme, implementing such boundary conditions requires special attention, as boundary nodes must be incorporated directly into the interpolation system to ensure physical consistency.

3 Numerical Methods

3.1 Formulation of the RBF Differentiation Operators

To address the numerical solution of the governing equations, we use the RBF method, an innovative mesh free approach proposed by Kansa [14]. Herein, we proceed to delineate the key attributes of this method [15].

The essence of the RBF interpolation lies in approximating the solution function using an expansion. Following the Kansa method, this involves approximating the solution at a set of $S_N = \{(x_i, y_i)\}_{i=1,N}$ collocation nodes. This approximation is achieved by combining radial basis functions in a linear manner, as expressed below [25]:

$$f(x,t) = \sum_{j \in s_N} \lambda_{F,j} \phi\left(\left\|x - x_i\right\|, \varepsilon\right) \tag{6}$$

The approach involves determining the unknown coefficients $\lambda_{F,j}$ with $\Phi(x)$ representing a radial basis function and $\|x - xj\|$ denoting the distance between nodes x and xj. The literature presents various radial basis functions, among which the smoothly infinite multiquadric radial basis function is employed in this study. This function is defined as $\phi\left(\left\|x - x_i\right\|\right) = \sqrt{1 - \varepsilon\left\|x - x_i\right\|^2}$, In this context, $\varepsilon \neq 0$ shape parameter, plays a critical role in improving accuracy. The optimal range of shape values is determined through numerical tests, including the procedure proposed by Sarra in [25], which aids in identifying an appropriate shape parameter. Throughout the simulations, we maintain ε_0 within the range of $10^{-4} \leq \varepsilon_0 \leq 2\times10^{-1}$, with ε_0 chosen as the smallest value for which $\varepsilon = \varepsilon_0 \frac{\sqrt{n}}{d_{\min}}$, where d_{min} signifies the minimum node distance. For tackling equations involving partial derivatives in their numerical solution, we resort to a linear approximation strategy. This entails the estimation of partial derivatives at the x nodes by utilizing RBF, and the procedure is depicted as follows:

$$Lf(x,t) = \sum_{j \in s_{i,n}} \lambda_{F,j} L\phi\left(\left\|x - x_j\right\|, \varepsilon\right) \tag{7}$$

This can be restated more succinctly as:

$$Lf = \phi_L \Lambda_f \tag{8}$$

In this context, Λ_f represents a vector of coefficients with dimensions N × 1 to be determined, and ϕ_L is an N × N matrix that encompasses the linear differentiation of the radial basis function $L\phi\left(\left\|x_i - x_j\right\|, \varepsilon\right)$. By employing Equ. (6), we can formulate the coefficients Λ_f with respect to the function F as follows:

$$\Lambda_f = (\phi)^{-1} f \tag{9}$$

Here, $(\phi)^{-1}$ stands for the matrix $\Phi^{'}$s inverse. Simplifying the equation by eliminating the reliance on the expansion coefficients, Equ. (8) transforms into:

$$Lf = \phi_L (\phi)^{-1} f \tag{10}$$

By adopting this approach, we can articulate the initial and secondary spatial derivatives of a function f (x, t) as follows:

$$\frac{\partial f(x,t)}{\partial x} = M_x f(x,t); \frac{\partial f(x,t)}{\partial y} = M_y f(x,t); \tag{11}$$

$$\frac{\partial^2 f(x,t)}{\partial x^2} = M_{xx} f(x,t) \; and \; \frac{\partial^2 f(x,t)}{\partial y^2} = M_{yy} f(x,t) \tag{12}$$

In this regard, $M_x, M_y, M_{xx}, and\, M_{yy}$ represent matrices encompassing the first and second derivatives concerning x and y.

3.2 Computational Technique

In this section, we move forward to describe the execution of the LRBF (Local Radial Basis Function) method for simultaneously handling the shallow water equations and the convection-diffusion equation involving a non-active pollutant. To start, we choose a set of N distinct points within the study area. Equ. (1) will then be approximated by the following equivalent system:

$$\partial_t W = -F'(W) - G'(W) + S'_b(W) + S_f(W) \tag{13}$$

In this context, F' and G' represent the convective flux and S'_b accounts for variations at the bottom. By performing numerical evaluation using the LRBF mesh free method, the outcome is as follows:

$$F'(W)=\begin{bmatrix} M_x q_x \\ M_x(\frac{q_x^{\,2}}{h}+\frac{1}{2}gh^2) \\ M_x(\frac{q_x q_y}{h}) \end{bmatrix}, G'(W)=\begin{bmatrix} M_y q_y \\ M_y(\frac{q_x q_y}{h}) \\ M_y(\frac{q_y^{\,2}}{h}+\frac{1}{2}gh^2) \end{bmatrix}, S'_b=\begin{bmatrix} 0 \\ -ghM_x z \\ -ghM_y z \end{bmatrix} \tag{14}$$

Therefore, the numerical solution entails the iterative computation of all the relevant derivatives, a process that occurs multiple times within a single time step. To ensure computational efficiency, we employ a sequence in which we initially compute the derivative matrices $M_x, M_y, M_{xx}, and\ M_{yy}$, and subsequently, we evaluate the numerical fluxes.

For time advancement, we utilize the second-order Runge-Kutta method is used for approximating the temporal derivative in the hydraulic jump problem, this decision is justified by its ability to provide a middle ground between computational efficiency and accuracy. This choice offers improved accuracy over first-order schemes while being less computationally demanding than higher-order alternatives. In the context of the hydraulic jump's complex dynamics, the scheme's accuracy in tracking time-dependent variables is advantageous. Its straightforward implementation makes it suitable for practical application, and its temporal stability is noteworthy, especially for capturing rapid variations in hydraulic jump dynamics without introducing numerical instability. In summary, the second-order Runge-Kutta scheme is a balanced and well-suited approach for effectively representing temporal changes in the hydraulic jump problem's differential equations. The equation employed for computing the solution W^{n+1} at the (n + 1) time level is as follows:

$$\begin{aligned} W^{n+1} &= \frac{1}{2}(W^n + W^*) - \frac{\Delta t}{2}\left[F'(W^*) + G'(W^*) - S'_b(W^*) - S_f(W^*)\right] \\ W^* &= W^n - \Delta t\left[F'(W^n) + G'(W^n) - S'_b(W^n) - S_f(W^n)\right] \end{aligned} \tag{15}$$

Within the aforementioned equation, Δt denotes the time step, the selection of which requires careful consideration to ensure scheme stability. Throughout all our simulations, we determine Δt employing the subsequent formula:

$$\Delta t = CFL\frac{d_{\min}}{\max\left(\left|\frac{q_x}{h}\right|,\left|\frac{q_y}{h}\right|\right)} \tag{16}$$

In this formula, d_{min} signifies the smallest distance between nodes, and the CFL number (Courant-Friedrichs-Lewy) is set at 0.5. At the outset of each step within the Runge-Kutta (RK) scheme, the assessment of the friction effect takes place and is employed implicitly through the splitting scheme introduced in [16]. By considering only the local acceleration and bed friction terms, we approximate the momentum equation as follows:

$$\frac{dW}{dt} = S_f^{n+1} \tag{17}$$

As the friction term solely impacts the momentum equation, it is necessary to evaluate only the flow rates. Consequently, the subsequent implicit scheme is employed [9]:

$$q_i^{n+1} = q_i^n + \frac{\Delta t S_f}{1 - 2\Delta t S_f \left(q_i^n\right)^{-1}} \tag{18}$$

This modified flux is employed as an initial condition for the operators in the Equ. (15).

3.3 Artificial Viscosity Based RBF Stabilization

It is widely recognized that discretizing the SWEs, particularly in scenarios dominated by the convection term, can result in non-physical oscillations. As illustrated in various studies [17], a viable solution to counter this issue involves introducing an artificial viscosity, referred to as hyperviscosity, into the system's second component. This hyperviscosity serves as a filter, functioning subsequently:

$$\partial_t W = RHS(W) + \gamma \Delta^k W \tag{19}$$

Here, k represents the order of the Laplacian operator. By utilizing the RBF approximation method outlined earlier, the artificial viscosity operator is represented by the ensuing expression:

$$\gamma \Delta^k W = \gamma M_{\Delta^k} W \tag{20}$$

In the given equation, γ signifies the viscosity to be introduced, which is also referred to as the damping coefficient. As discussed in [17], various approaches exist to determine the optimal value for gamma. To maintain both stability and accuracy, the values of gamma are directly associated with the grid's resolution and the order k [18]. Nevertheless, the most straightforward technique involves trial and error through short tests.

4 Numerical Results and Discussions

To validate the proposed MQ-RBF meshless solver with artificial viscosity, three benchmark problems were studied: (i) the oblique hydraulic jump in a contracting channel, (ii) supercritical flow in a converging channel, and (iii) a transcritical flow over an irregular bottom topography. These problems are well established in the hydraulic literature [21–27] and provide rigorous tests of both shock resolution and numerical stability.

4.1 Oblique Hydraulic Jump over Flat Bottom

An oblique hydraulic jump occurs when a supercritical flow encounters a contraction, producing an inclined shock front. The computational domain, node distribution (**Fig.1**), and inflow conditions (h=1 m, u=9 m/s, v=0) follow [7]. **Fig.2** shows the two-

and three-dimensional distributions of the computed water depth. The oblique shock front is clearly visible, aligning with physical expectations of momentum conservation under channel contraction.

Fig.3 compares the longitudinal water depth profile along y=2 with the reference solution from Li et al. [7]. The present MQ-RBF scheme reproduces both the location and magnitude of the jump with high fidelity. This agreement demonstrates that the artificial viscosity successfully damps oscillations at the discontinuity without blurring the shock front. Physically, the method captures the sudden conversion of kinetic energy into turbulence and localized depth increase, which characterizes hydraulic jumps.

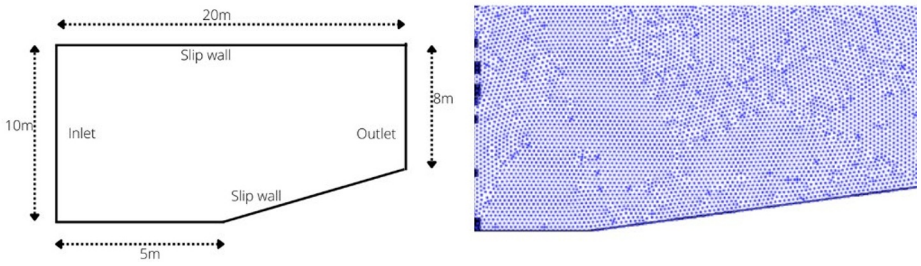

Fig.1. Geometry of study area and computational nodes.

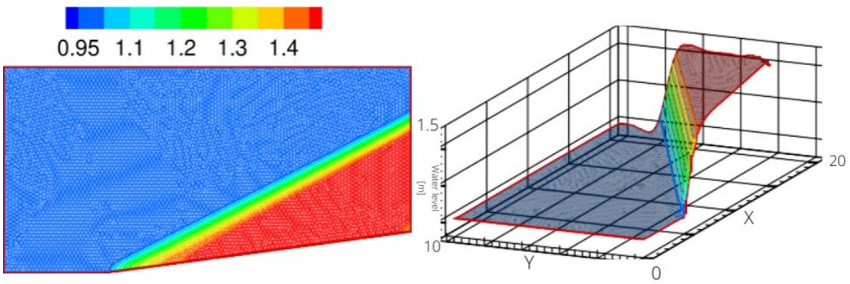

Fig.2. Visualizing the numerical solutions of water level h in both 2D and 3D plots.

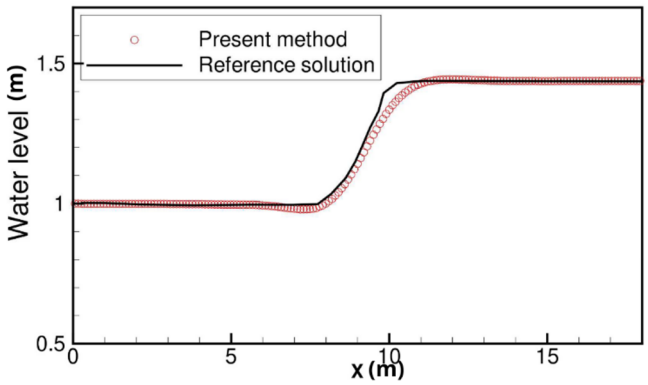

Fig. 1. Numerical solution of water level (*h*) using the present method compared with a reference solution along $y = 2$.

4.2 Supercritical Flow over a Converging Channel

The second case examines supercritical flow through a narrowing cross-section, another classic configuration leading to shock interactions [7], [21]. The results in **Fig.5** and **Fig.6** show that two shock waves form symmetrically as the contraction intensifies, leading to depth variations consistent with experimental observations.

Fig.7 compares the computed water depth along y=0.3145 with experimental data from Bhallamudi and Chaudhry [21] and numerical results from other authors[7], [22]. The MQ-RBF scheme not only matches the reference trends but also reproduces the sharp transitions in water depth, confirming the robustness of the artificial viscosity formulation. Physically, the contraction accelerates the flow, generating shocks that restore momentum balance; the solver successfully tracks these rapid nonlinear adjustments.

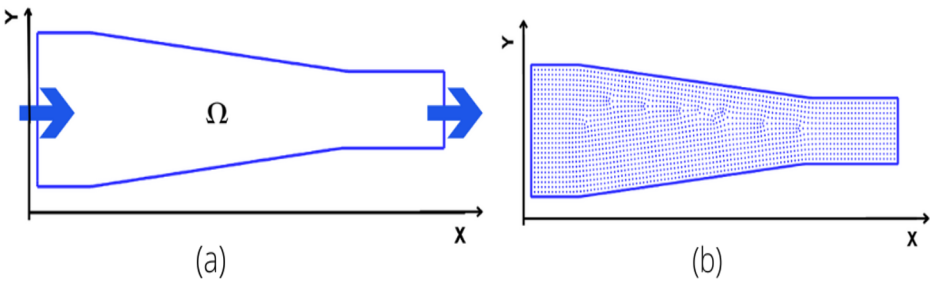

Fig.4. (a) Schematic diagram of the computational domain, and (b) Distribution of nodes used for the problem in the converging channel.

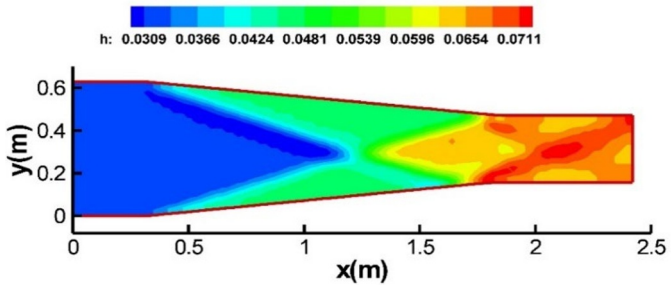

Fig.5. Plotting the 2D numerical solutions of water depth h.

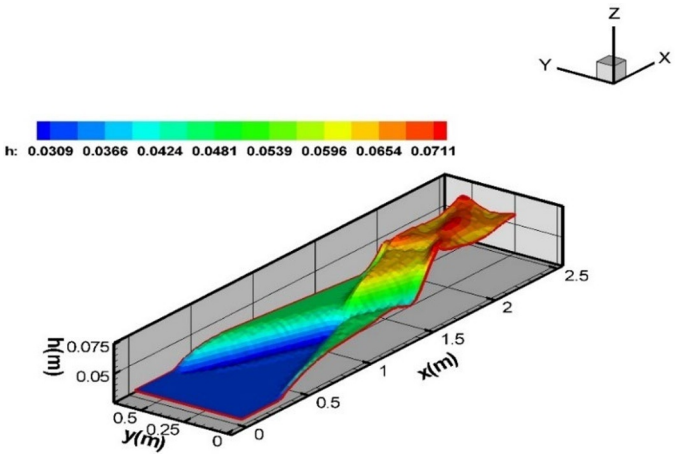

Fig.6. Plotting the 3D numerical solutions of water depth h.

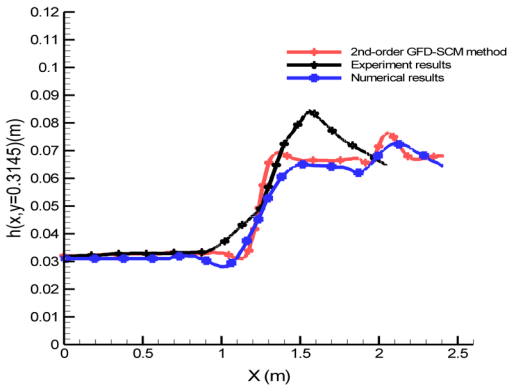

Fig.7. Visualizing the distributions of water depth h at y = 0.3145 using various methods.

4.3 Hydraulic Jump over Irregular Bottom

The third test evaluates the method's ability to capture shocks induced by bed topography variations. The bottom profile is given by Eq. (21), representing a hump centered in the channel. Under a prescribed upstream discharge of 0.18 $m^2.s^{-1}$ and downstream depth of 0.33m, a transcritical flow develops with a stationary jump downstream of the hump.

$$z(x,y)=\begin{cases}0.2-0.05(x-10)^2 & if\ \ 0\le x\le 12m\\ 0 & otherwise\end{cases} \tag{21}$$

And with the following initial conditions:

$$\begin{cases} h(x,y,t=0)=2-z(x,y)\\ q_x(x,y,t=0)=q_y(x,y,t=0)=0\end{cases} \tag{22}$$

Fig.9 presents a three-dimensional visualization of the free surface and bed elevation. The formation of a localized hydraulic jump is evident, while **Fig.10** compares longitudinal water depth profiles with analytical predictions [23], [24]. The proposed method reproduces the position and magnitude of the shock with high accuracy. This confirms that the artificial viscosity effectively handles topography-induced source terms without destabilizing the solution. Physically, the stationary shock arises from the inability of the flow to remain supercritical over the bed hump, forcing a transition to subcritical conditions accompanied by energy dissipation. The solver captures this balance between gravitational forcing and bed resistance.

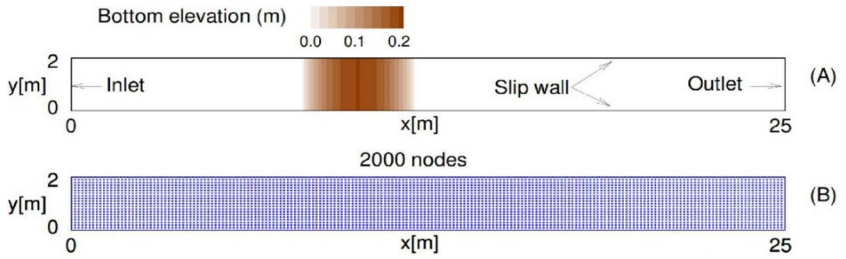

Fig.8. Schematic diagram and computational nodes used for the problem of a hydraulic jump.

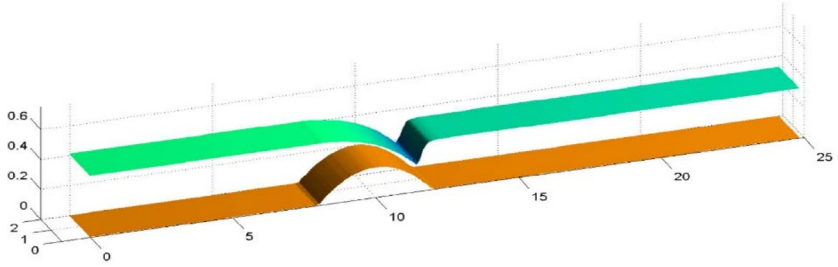

Fig.9. Three-dimensional view of water level and bed shape.

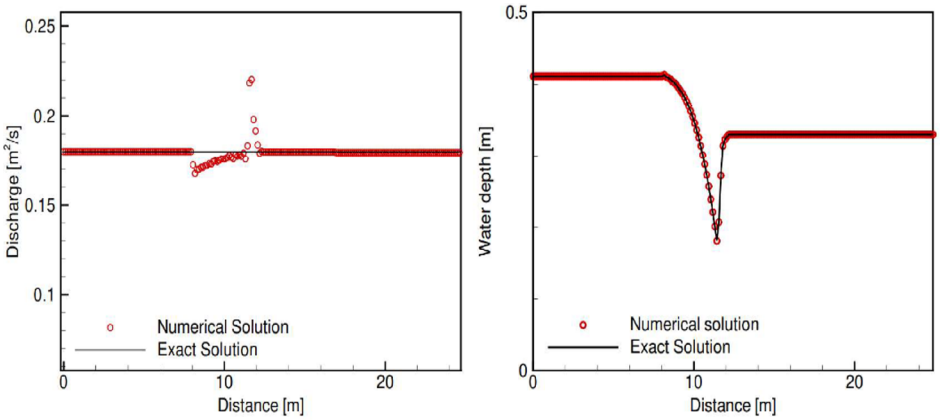

Fig.10. Comparison between a longitudinal section of water level and flow as well as analytical solutions.

4.4 Discussion

Across all three cases, the MQ-RBF solver demonstrates strong agreement with analytical, experimental, and numerical reference solutions [21–27]. Importantly, the method not only provides quantitative accuracy but also captures the **physical mechanisms** underlying shock formation:

- **Momentum redistribution** at contractions (oblique jumps).
- **Symmetric shock generation** under flow acceleration in converging channels.
- **Topography-induced transitions** from supercritical to subcritical regimes (irregular bottom).

The artificial viscosity formulation proves essential, eliminating spurious oscillations while retaining shock sharpness. Compared with traditional finite volume approaches [3–8], the meshless framework avoids mesh generation and remains efficient for complex geometries. These findings highlight the potential of MQ-RBF methods as practical alternatives for shock-resolved shallow water modeling.

5 Conclusions

This study presented a meshless framework for solving the two-dimensional shallow water equations using multiquadric radial basis functions (MQ-RBFs) combined with an artificial viscosity stabilization strategy. The method addresses two key challenges: suppressing spurious oscillations near shocks and retaining the high accuracy characteristic of RBF-based collocation. Time integration with a second-order Runge–Kutta scheme provided a good compromise between accuracy and efficiency.

The solver was validated against three benchmark cases: the oblique hydraulic jump, supercritical flow through a converging channel, and transcritical flow over a variable bed. In each scenario, the MQ-RBF model reproduced the location, magnitude, and physical behavior of hydraulic shocks in close agreement with analytical solutions, experimental data, and established numerical results [21–27]. The physical interpretation of results confirmed that the method captures essential flow dynamics such as momentum redistribution at contractions, symmetric shock formation in accelerating channels, and stationary jumps induced by topography.

The novelty of this work lies in extending MQ-RBF methods with artificial viscosity to shock-resolved SWE problems, demonstrating that a meshless approach can perform competitively with classical finite volume solvers while avoiding mesh generation and connectivity constraints. This positions the method as a promising alternative for complex hydraulic applications where irregular domains or moving boundaries make mesh-based schemes less practical.

Future research will focus on extending the approach to unsteady wet–dry transitions, optimizing the viscosity formulation, and exploring applications to large-scale environmental flow simulations.

References

[1] P. Glaister, « A numerical scheme for two-dimensional, open channel flows with non-rectangular geometries », *Int. J. Eng. Sci.*, vol. 31, nº 7, p. 1003-1011, juill. 1993, doi: 10.1016/0020-7225(93)90108-7.

[2] P. Glaister, « Prediction of steady, supercritical, free-surface flow », *Int. J. Eng. Sci.*, vol. 33, nº 6, p. 845-854, mai 1995, doi: 10.1016/0020-7225(94)00095-2.

[3] K. S. Erduran, V. Kutija, et C. J. M. Hewett, « Performance of finite volume solutions to the shallow water equations with shock-capturing schemes », *Int. J. Numer. Methods Fluids*, vol. 40, nº 10, p. 1237-1273, déc. 2002, doi: 10.1002/fld.402.

[4] D. H. Zhao, H. W. Shen, G. Q. Tabios, J. S. Lai, et W. Y. Tan, « Finite-Volume Two-Dimensional Unsteady-Flow Model for River Basins », *J. Hydraul. Eng.*, vol. 120, nº 7, p. 863-883, juill. 1994, doi: 10.1061/(ASCE)0733-9429(1994)120:7(863).

[5] K. S. Erduran, V. Kutija, et C. R. Macalister, « Finite volume solution to integrated shallow surface-saturated groundwater flow », *Int. J. Numer. Methods Fluids*, vol. 49, nº 7, p. 763-783, nov. 2005, doi: 10.1002/fld.1030.

[6] S. Chippada, C. N. Dawson, M. L. Martinez, et M. F. Wheeler, « A Godunov-type finite volume method for the system of Shallow water equations », *Comput. Methods Appl. Mech. Eng.*, vol. 151, nº 1-2, p. 105-129, janv. 1998, doi: 10.1016/S0045-7825(97)00108-4.

[7] P.-W. Li, C.-M. Fan, et J. K. Grabski, « A meshless generalized finite difference method for solving shallow water equations with the flux limiter technique », *Eng. Anal. Bound. Elem.*, vol. 131, p. 159-173, oct. 2021, doi: 10.1016/j.enganabound.2021.06.022.

[8] K. Hu, C. G. Mingham, et D. M. Causon, « A bore-capturing finite volume method for open-channel flows », *Int. J. Numer. Methods Fluids*, vol. 28, nº 8, p. 1241-1261, nov. 1998, doi: 10.1002/(SICI)1097-0363(19981130)28:8<1241::AID-FLD772>3.0.CO;2-2.

[9] E. Chaabelasri, « Numerical Simulation of Dam Break Flows Using a Radial Basis Function Meshless Method with Artificial Viscosity », *Model. Simul. Eng.*, vol. 2018, p. 1-11, 2018, doi: 10.1155/2018/4245658.

[10] P.-W. Li et C.-M. Fan, « Generalized finite difference method for two-dimensional shallow water equations », *Eng. Anal. Bound. Elem.*, vol. 80, p. 58-71, juill. 2017, doi: 10.1016/j.enganabound.2017.03.012.

[11] N.-J. Wu, C. Chen, et T.-K. Tsay, « Application of weighted-least-square local polynomial approximation to 2D shallow water equation problems », *Eng. Anal. Bound. Elem.*, vol. 68, p. 124-134, juill. 2016, doi: 10.1016/j.enganabound.2016.04.010.

[12] Y.-C. Hon, K. F. Cheung, X.-Z. Mao, et E. J. Kansa, « Multiquadric Solution for Shallow Water Equations », *J. Hydraul. Eng.*, vol. 125, nº 5, p. 524-533, mai 1999, doi: 10.1061/(ASCE)0733-9429(1999)125:5(524).

[13] B. Marwane et C. Elmiloud, « Numerical solution by meshless method of a fully-coupled bed load and shallow water flows », *E3S Web Conf.*, vol. 336, p. 00003, 2022, doi: 10.1051/e3sconf/202233600003.

[14] E. J. Kansa, « Multiquadrics—A scattered data approximation scheme with applications to computational fluid-dynamics—I surface approximations and partial derivative estimates », *Comput. Math. Appl.*, vol. 19, nº 8-9, p. 127-145, 1990, doi: 10.1016/0898-1221(90)90270-T.

[15] M. Al Nuwairan et E. Chaabelasri, « Balanced Meshless Method for Numerical Simulation of Pollutant Transport by Shallow Water Flow over Irregular Bed: Application in the Strait of Gibraltar », *Appl. Sci.*, vol. 12, nº 14, p. 6849, juill. 2022, doi: 10.3390/app12146849.

[16] E. Chaabelasri, M. Jeyar, et A. G. L. Borthwick, « Explicit radial basis function collocation method for computing shallow water flows », *Procedia Comput. Sci.*, vol. 148, p. 361-370, 2019, doi: 10.1016/j.procs.2019.01.044.

[17] B. Fornberg et E. Lehto, « Stabilization of RBF-generated finite difference methods for convective PDEs », *J. Comput. Phys.*, vol. 230, nº 6, p. 2270-2285, mars 2011, doi: 10.1016/j.jcp.2010.12.014.

[18] N. Flyer, E. Lehto, S. Blaise, G. B. Wright, et A. St-Cyr, « A guide to RBF-generated finite differences for nonlinear transport: Shallow water simulations on a sphere », *J. Comput. Phys.*, vol. 231, nº 11, p. 4078-4095, juin 2012, doi: 10.1016/j.jcp.2012.01.028.

[19] S. N. Kuiry, K. Pramanik, et D. Sen, « Finite Volume Model for Shallow Water Equations with Improved Treatment of Source Terms », *J. Hydraul. Eng.*, vol. 134, nº 2, p. 231-242, févr. 2008, doi: 10.1061/(ASCE)0733-9429(2008)134:2(231).

[20] S. Murty Bhallamudi et M. Hanif Chaudhry, « Computation of flows in open-channel transitions », *J. Hydraul. Res.*, vol. 30, nº 1, p. 77-93, janv. 1992, doi: 10.1080/00221689209498948.

[21] T. Molls et M. H. Chaudhry, « Depth-Averaged Open-Channel Flow Model », *J. Hydraul. Eng.*, vol. 121, nº 6, p. 453-465, juin 1995, doi: 10.1061/(ASCE)0733-9429(1995)121:6(453).

[22] X. Ying et S. S. Y. Wang, « Improved implementation of the HLL approximate Riemann solver for one-dimensional open channel flows », *J. Hydraul. Res.*, vol. 46, nº 1, p. 21-34, janv. 2008, doi: 10.1080/00221686.2008.9521840.

[23] Y. Xing, « High order finite volume WENO schemes for the shallow water flows through channels with irregular geometry », *J. Comput. Appl. Math.*, vol. 299, p. 229-244, juin 2016, doi: 10.1016/j.cam.2015.11.042.

[24] G. Yao, C. S. Chen, W. Li, et D. L. Young, « The localized method of approximated particular solutions for near-singular two- and three-dimensional problems », *Comput. Math. Appl.*, vol. 70, nº 12, p. 2883-2894, déc. 2015, doi: 10.1016/j.camwa.2015.09.028.

[25] S. A. Sarra, « A local radial basis function method for advection–diffusion–reaction equations on complexly shaped domains », *Appl. Math. Comput.*, vol. 218, nº 19, p. 9853-9865, juin 2012, doi: 10.1016/j.amc.2012.03.062.